Smart Mater. Struct. 1 (1992) 214–226. Printed in the UK

Active plate and wing research using EDAP elements

Ron Barrett

Aerospace Engineering Department, 2004 Learned Hall, University of Kansas, Lawrence, Kansas 66045-2221, USA

Received 8 June 1992, accepted for publication 17 June 1992

Abstract. The deflection characteristics of structures using directionally attached piezoelectric (DAP) and enhanced DAP (EDAP) elements are explored. Tests demonstrate that piezoceramic elements, which are isotropic, exhibit orthotropic behavior when directionally attached using any of three methods: (i) partial attachment, (ii) transverse shear lag, and (iii) differential stiffness bonding. Test results demonstrate that directional enhancement through transverse stiffening can increase DAP element strain from 5 to 25%. Closed form expressions of DAP/EDAP strains based on classical laminated plate theory are presented. The models demonstrate that DAP/EDAP elements generate any in-plane strain (extensions and shear) or out-of plane curvature (bending in either direction and twist) independent of other strains or curvatures. Test results show that fiberglass and aluminium DAP/EDAP beams produce torsional and bending deflections in excess of $30° m^{-1}$ with theory and experiment in close agreement. The deflections of DAP/EDAP and conventional piezoelectric active structures are compared. Tests show that DAP/EDAP elements can produce up to 16 times more twist than conventionally attached piezoceramic elements. Two wings were constructed with DAP and EDAP elements. EDAP elements were laminated into the skin of a graphite/epoxy supersonic wing that had a 9% thick diamond airfoil section and an aspect ratio of 3. DAP elements were also laminated to a torsion beam of a subsonic wing that had an NACA 0012 profile and an aspect ratio of 1.4. The supersonic wing demonstrated static twist deflections in excess of 2°. The subsonic wing demonstrated static pitch deflections of 9°. The lifting capability of the DAP/EDAP wings are compared to piezo-ailerons. The DAP/EDAP wings are shown to produce much larger changes in lift coefficient and greater deflection stability with increasing airspeed than the piezo-aileron configuration.

1. Introduction

Adaptive structures that move in bending and extension have been investigated and successfully modeled by numerous experimenters. Crawley and Anderson [1], Kinsley *et al* [2] and Hanagud [3] modeled the behavior of active plates with PZT elements in bending and extension. Improvements to Euler and plate theory models have added to the prediction capability. Crawley and De Luis [4] included shear lag and stress analyses in their dynamic performance estimations of active beams using piezoceramic actuator elements. To control active structures with masses placed off the elastic axis or in twist modes, manipulation of the structural twist as well as independent bending control is necessary. Until recently, no investigator has used active bending and twist control because no usable shear-capable piezoceramic elements (possessing a d_{36} property) have been commercially available. Only piezoelectric polymers like PVDF have exhibited this property when laminated at off-axis angles. For aerodynamic applications, active twist control is highly desirable, but the lack of a d_{36} capable piezoceramic has prevented this structural manipulation. Crawley and co-workers [5, 6] worked on the problem of structural twist manipulation with extension-twist and bending-twist coupled plates. The plates were bent or extended by the PZT elements to induce twist deflections of the order of 1 to 3 degrees. One test conducted by Crawley, Lazarus and Warkentin investigated the new field of aeroservoelasticity when they placed a bending-twist coupled plate in a wind tunnel and actively bent it by piezoceramic elements. They showed that airloads could be used to further twist the wing and effectively double or triple the amount of lift generated. Unfortunately, the high degree of bending-twist coupling necessary to produce these deflections meant that any wing that used this method could not be optimized for strength and would eventually suffer from forms of divergence. Other researchers sought ways of generating torsional shear flows without relying upon structural coupling. Garcia [7] used the small amount of shear generation capability that is obtained from the d_{15} shear charge coefficient. He

0964-1726/92/030214 + 13 $07.50

showed that very small amounts of twist could be generated by PZT elements in materials with tubular cross-sections. Accordingly, difficulties were encountered because extremely high charges were required for d_{15} activation. This method is currently shown to be infeasible for plate and wing actuation. Another approach to generating torsional deformations with negligible structural coupling used a completely different approach. Barrett [8–12] and Chopra [13] showed that isotropic PZT actuator elements could be given orthotropic characteristics through directional attachment. These directionally attached piezoelectric (DAP) elements were laminated at off-axis angles to generate torsional shear flows. Directional attachment artificially induced a d_{36} capability in piezoceramic elements that would otherwise be shear-inactive and made both shear and twist activation possible. DAP elements were used to twist uncoupled plates and aerodynamic surfaces with significantly higher deflections than those generated by other techniques, including those tried by Crawley *et al* [5]. The DAP elements were laminated in rotor blades, rotor blade torque tubes and wings, demonstrating that air loads could be significantly manipulated. Spangler and Hall [14] also explored the manipulation of air loads through PZT bender elements. They used a conventional aileron manipulated by a bimorph PZT beam, actuated in bending. Significant deflections were generated and data was presented on frequency response, frictional effects and deflection degradation under air loads. A change in lift coefficient in excess of 0.15 was demonstrated by the wing section, and was intended to be used as a rotor blade servotab section. The extrapolated data shows that the adverse flap hinge moment generated by air loads overpowers the bimorph bender elements at speeds as low as $20\,\mathrm{m\,s^{-1}}$. At $50\,\mathrm{m\,s^{-1}}$ the control authority was shown to degrade by more than an order of magnitude.

The main objectives of this investigation are to lay out the properties of DAP and EDAP elements both experimentally and analytically and to explore methods of integrating them in missile wings so that the difficulties experienced by previous investigators (like control power degradation and adverse coupling) may be alleviated.

2. Analysis of DAP and EDAP elements

Three steps are taken to effectively model DAP and EDAP elements. The first step establishes the longitudinal and lateral stiffnesses of the DAP element in the DAP ply. This first step takes into account the effects of the three methods of directional attachment. The second step is to model directional enhancement and to estimate the increase in EDAP strain that is available from directional enhancement. The final step is to integrate the stiffnesses and activator strains into plate models so the behavior of the laminate can be predicted. Figures 1(*a*), (*b*), and (*c*) outline the fundamentals of each method. In practice, all three methods of directional attachment are used simultaneously for best results. Each method provides the DAP element with increasing orthotropy, and allows the element to perform with minimal warping and strong resistance to de-bonds.

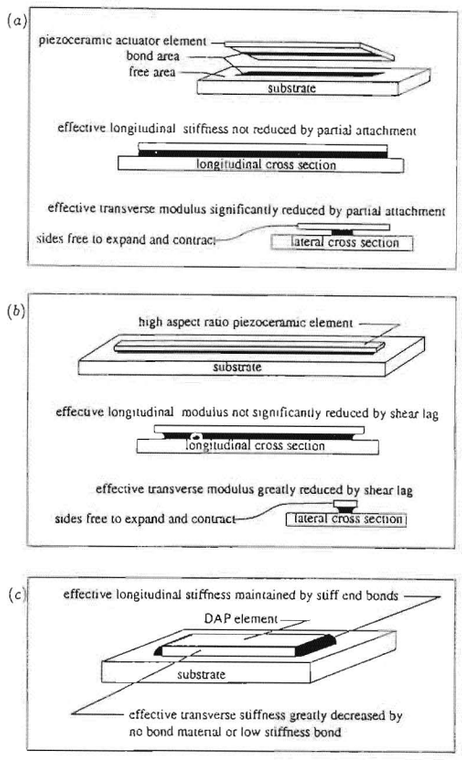

Figure 1. Directional attachment method: (*a*) partial attachment; (*b*) transverse shear lag; (*c*) differential stiffness bonding.

Directional attachment through partial attachment gives the element a high degree of orthotropy and is amenable to surface lamination or embedding. In early stages of experimentation, stress concentrations at the ends of the element caused frequent de-bonds [8]. Tailoring of the attachment area and differential stiffness attachment have since alleviated this problem.

The models of directional attachment through partial attachment take into account the geometry of the bond. The following models adjust the effective stiffnesses of the element and assume that the bonding strip extends approximately the complete length of the element and only part of the width of the element. These new stiffness modification models improve upon earlier models which could only account for rectangular attachment areas [8–13].

$$E_{L\mathrm{eff}o} = E_{Lo}\left(\frac{L_{\mathrm{eff}o}}{L_o} - \frac{(W_o - W_{\mathrm{eff}o})^2}{2L_o W_o}\right) \tag{1}$$

$$E_{T\mathrm{eff}o} = E_{To}\int_0^{Lo} \frac{W_{\mathrm{eff}o}(x)}{W_o L_o}\,\mathrm{d}x. \tag{2}$$

The transverse and longitudinal stiffnesses of the DAP actuator ply are modified by the geometry of the element to account for the partial attachment. Figure 2 shows a cross section of a DAP element. Partial attachment is

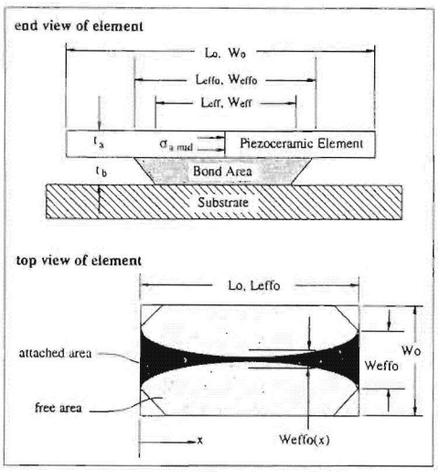

Figure 2. Bond geometry of DAP element.

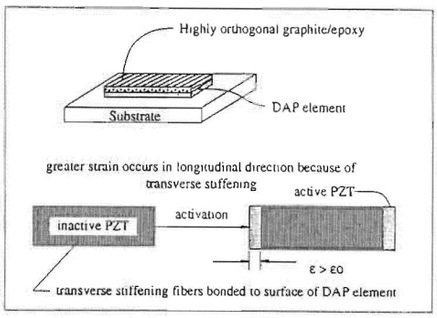

Figure 3. Fundamental arrangement of directionally enhanced piezoelectric element.

normally carried out in the transverse direction so as to reduce the transverse stiffness, but the longitudinal direction may also experience some partial attachment from various manufacturing procedures. From the top view of figure 2, the gray area represents the amount of elemental area that does work in the longitudinal direction, and the white triangles at the corners of the DAP element do relatively little work in the longitudinal direction. This has been demonstrated experimentally by Barrett [8].

The second method of achieving directional attachment is through transverse shear lag. Shear lag reduces the effective transverse stiffness of the DAP element by allowing it to strain laterally with little restriction. Longitudinally, the shear lag is minimal with respect to the total element length, and the longitudinal strain transmission to the substrate is maintained. Like partial attachment, transverse shear lag is dependent upon element geometry and attachment area geometry. Transverse shear lag is also a function of the thickness and stiffness of the bond material. It can be seen that the higher the aspect ratio, the greater the orthotropy. Equation (3) shows that the original effective modulus, $E_{L\text{effo}}$, can be modified to obtain the effective modulus by selecting the location on the DAP element where the element stress reaches 50% of the mid-plane stress. The presence of $E_{L\text{effo}}$ in equation (3) indicates that it is useful for estimating the performance of both rectangular and irregularly shaped attachment areas.

$$\frac{E_{L\text{eff}}}{E_{L\text{effo}}} = \frac{\sinh^{-1}[\frac{1}{2}\sinh(\frac{1}{2}L_{\text{effo}}\sqrt{G_b/t_a t_b E_a})]}{\frac{1}{2}L_{\text{effo}}\sqrt{G_b/t_a t_b E_a}}. \qquad (3)$$

The effective transverse stiffness is obtained by substituting the original effective widths for lengths in equation (3). The DAP effective shear modulus $G_{LT\text{eff}}$ is obtained by using the same procedures that yield the effective longitudinal stiffness.

Directional attachment through differential stiffness bonding is much more difficult to model as the end and side fixities are dependent upon many variables. In general, the purpose of end-bonding has been to reduce the large stress concentrations in the shear attachment. Accordingly, end-bonding makes the DAP element more resistant to de-bonds. End bonding alone is not normally used because the elements easily warp and buckle when in compression. When in tension, the elements tend to fail at the bond juncture. End bonding works well when used with partial attachment as the element is attached strongly in shear and prevented from buckling. The net effect of stiff end bonding is to increase to orthotropy of the element so that $E_{L\text{eff}}/E_{L\text{o}} \simeq \text{SL}_{\text{effo}}/L_{\text{o}} \simeq 1$.

To account for directional attachment in laminated plate theory, the effective stiffnesses are used where the longitudinal and transverse stiffnesses would be applied.

3. Modeling directional enhancement

The enhancement of DAP elements is achieved by bonding very stiff fibers transversely on the DAP element with low modulus resin. Poisson's effect causes an increase in strain in the longitudinal direction and is schematically laid out in figure 3.

From classical laminated plate theory (CLPT), the amount of strain enhancement that can be obtained through transverse stiffening is modeled by assuming that the element encounters in-plane strains. Equation (4) shows this simple model which does not account for any curvatures:

$$\frac{(A_{22\text{l}} - A_{12\text{l}})(A_{11\text{a}} + A_{12\text{a}})\Lambda}{A_{11\text{l}}A_{22\text{l}} - A_{12\text{l}}^2} = \varepsilon_{11}. \qquad (4)$$

For ideal directional enhancement (transverse stiffness of fiber layer = ∞, longitudinal stiffness = 0) the longitudinal strain, ε_{11}, is approximately 33% greater than the original actuation strain.

To combine the effects of directional attachment and directional enhancement, a first method of approximation indicates that ε_{11} of equation (4) can be substituted in equation (10) for the actuation strain, Λ. This will yield an increase in all laminate strains in proportion to the effectiveness of the directional enhancement.

3.1. Classical laminated plate theory models

Classical laminated plate theory (CLPT) models are used to model the behavior of conventionally attached piezoceramic (CAP), DAP, and EDAP elements. The CLPT analysis and formulation follows the normal assumptions laid out in Jones [15]. The elements may be surface bonded or embedded in the structure in any sequence, actuated in extension or contraction and oriented at any angle. The in-plane strain components are assumed constant through the thickness and the strains caused by bending are assumed to be linearly varying through the thickness of the plate.

Crawley and Lazarus [6] and Barrett [9, 10] use the formulation that Jones [15] employs for modeling thermally induced strains in lamina. These active strains can be cast in terms of the mid-plane strains and curvatures in laminate axes:

$$\varepsilon = \begin{Bmatrix} \varepsilon^0 \\ \kappa \end{Bmatrix} = \begin{Bmatrix} \varepsilon_{11} \\ \varepsilon_{22} \\ \varepsilon_{12} \\ \kappa_{11} \\ \kappa_{22} \\ \kappa_{12} \end{Bmatrix} = \begin{Bmatrix} \partial u/\partial x \\ \partial v/\partial y \\ \tfrac{1}{2}(\partial u/\partial y + \partial v/\partial x) \\ -(\partial^2 w/\partial x^2) \\ -(\partial^2 w/\partial y^2) \\ -(\partial^2 w/\partial x \partial y) \end{Bmatrix}. \tag{5}$$

Following Jones [15], the interaction between the externally applied forces and moments, the laminate stiffness and the actuation strain induced forces and moments follow:

$$\begin{Bmatrix} N \\ M \end{Bmatrix} = \begin{bmatrix} A & B \\ B & D \end{bmatrix}_1 \begin{Bmatrix} \varepsilon^0 \\ \kappa \end{Bmatrix} - \begin{Bmatrix} N \\ M \end{Bmatrix}_a. \tag{6}$$

The stiffness matrix is composed of the reduced stiffnesses of each ply in the laminate axes. The applied forces and moments per unit length are integrated through the thickness of the plate and are defined accordingly

$$N = \int \sigma \, dz \quad M = \int \sigma z \, dz. \tag{7}$$

For the following examples, the plate will be unloaded and will be free on all edges. Accordingly, equation (6) can be expanded to show the actuation forces and moments

$$\begin{bmatrix} A & B \\ B & D \end{bmatrix}_1 \begin{Bmatrix} \varepsilon^0 \\ \kappa \end{Bmatrix} = \begin{Bmatrix} N \\ M \end{Bmatrix}_a = \begin{bmatrix} A & B \\ B & D \end{bmatrix}_a \begin{Bmatrix} \Lambda_\varepsilon \\ \Lambda_\kappa \end{Bmatrix}. \tag{8}$$

The differences between the CAP elements used by Crawley and Lazarus [6] and others will be contrasted with DAP/EDAP elements. DAP/EDAP elements are orthotropic while CAP elements are isotropic. This orthotropy allows them to be much more versatile than CAP elements and generate much larger strains and curvatures.

The strain actuation vector and the actuator stiffness matrix for conventionally attached piezoceramic elements take the form of equation (9). From Kinsley *et al* [2] the strains Λ_{31} and Λ_{32} are approximately the same for piezoceramics. If different actuator materials such as shape-memory alloys were employed, then the strain vector could be fully populated.

$$\begin{bmatrix} A & B \\ B & D \end{bmatrix}_a \begin{Bmatrix} \Lambda_\varepsilon \\ \Lambda_\kappa \end{Bmatrix} = \begin{bmatrix} A & B \\ B & D \end{bmatrix}_a \begin{Bmatrix} \Lambda_\varepsilon \\ 0 \end{Bmatrix} = \begin{Bmatrix} (A_{11} + A_{12})\Lambda \\ (A_{11} + A_{12})\Lambda \\ 0 \\ (B_{11} + B_{12})\Lambda \\ (B_{11} + B_{12})\Lambda \\ 0 \end{Bmatrix}_a. \tag{9}$$

From equation (9), for uncoupled substrates, it is obvious that only extensional strains, ε_{11}, ε_{22} and simple curvatures, κ_{11}, κ_{22} can be generated by the piezoceramic actuator elements. It is impossible to generate shear strain, ε_{12} and twist curvature, κ_{12}.

If the substrate is coupled, then all laminate extensions and curvatures may be generated. This coupling makes it impossible to control any given strain or curvature without exciting another strain or curvature. Table 1 outlines the substrate type, the types of strains and curvatures that may be generated by conventionally attached piezoceramic elements, and the strains and curvatures that are coupled to one another.

DAP elements do not suffer from this high degree of coupling because their orthotropy allows the actuation stiffness matrix to become fully populated. This fully populated stiffness matrix along with orthotropy ratios, OR, in excess of 100 allow DAP elements to generate any strain or curvature in coupled or uncoupled substrates without exciting other strains or curvatures. For DAP elements, the stiffness matrix becomes fully populated with all coupling terms as shown in equation (10),

$$\begin{bmatrix} A_{11} & A_{12} & 2A_{16} & B_{11} & B_{12} & 2B_{16} \\ A_{12} & A_{22} & 2A_{26} & B_{12} & B_{22} & 2B_{26} \\ A_{16} & A_{26} & 2A_{66} & B_{16} & B_{26} & 2B_{66} \\ B_{11} & B_{12} & 2B_{16} & D_{11} & D_{12} & 2D_{16} \\ B_{12} & B_{22} & 2B_{26} & D_{12} & D_{22} & 2D_{26} \\ B_{16} & B_{26} & 2B_{66} & D_{16} & D_{26} & 2D_{66} \end{bmatrix}_a \begin{Bmatrix} \Lambda \\ \Lambda \\ 0 \\ 0 \\ 0 \\ 0 \end{Bmatrix}$$

$$= \begin{Bmatrix} (A_{11} + A_{12})_a \Lambda \\ (A_{12} + A_{22})_a \Lambda \\ (A_{16} + A_{26})_a \Lambda \\ (B_{11} + B_{12})_a \Lambda \\ (B_{12} + B_{22})_a \Lambda \\ (B_{16} + B_{26})_a \Lambda \end{Bmatrix}. \tag{10}$$

Some experimenters have suggested that the actuation strain, Λ, should be altered to reflect unequal strains that may arise in the longitudinal and transverse directions of the DAP ply. If this alteration were included, then a strain vector including Λ_{31}, Λ_{32}, and Λ_{36} would be present. Experimentation has shown that corrections to the stiffnesses alone are enough to account for directional attachment.

Table 1. Coupled strains and curvatures that may be generated by CAP elements.

Substrate type (strains and curvatures that may be actuated)	Strains and curvatures generated	Coupled strains and curvatures
uncoupled	extension	ε_{11}, ε_{22}
(ε_{11}, ε_{22}, κ_{11}, κ_{22})	bending	κ_{11}, κ_{22}
	bending–extension	ε_{11}, ε_{22}, κ_{11}, κ_{22}
coupled	extension–twist	ε_{11}, ε_{22}, κ_{12}
(ε_{11}, ε_{22}, ε_{12}	extension–shear	ε_{11}, ε_{22}, ε_{12}
κ_{11}, κ_{22}, κ_{12})	bending–twist	κ_{11}, κ_{22}, κ_{12}
	bending–shear	κ_{11}, κ_{22}, ε_{12}
	bending–extension–twist	ε_{11}, ε_{22}, ε_{12} κ_{11}, κ_{22}, κ_{12}

3.2. Analysis of a symmetric 2-DAP ply laminate

Some structures call for the control of an uncoupled substrate in extension and twist without cross-feed of extension, ε_{11} to twist, κ_{12}. A symmetric laminate with a sequence of [+ΘDAP/uncoupled substrate/+ΘDAP] can control this substrate without cross-feed.

Extension activation is obtained by straining both DAP plies so that the laminate has the following structure: [+ΘDAP(+Λ)/uncoupled substrate/+ΘDAP(+Λ)]. For extensional activation, the laminate stiffness matrix of equation (6) and the actuator stiffness matrix of equation (10) collapse to a pair of 3 × 3 matrices

$$\begin{bmatrix} A_{11} & A_{12} & 2A_{16} \\ A_{12} & A_{22} & 2A_{26} \\ A_{16} & A_{26} & 2A_{66} \end{bmatrix}_a \begin{bmatrix} \Lambda \\ \Lambda \\ 0 \end{bmatrix}_a = \begin{bmatrix} A_{11} & A_{12} & 2A_{16} \\ A_{12} & A_{22} & 2A_{26} \\ A_{16} & A_{26} & 2A_{66} \end{bmatrix}_l \begin{bmatrix} \varepsilon_{11} \\ \varepsilon_{22} \\ \varepsilon_{12} \end{bmatrix}_l . \quad (11)$$

This indicates that the laminate experiences in-plane strains only without coupling to bending curvature.

Bending and twist activation is obtained by straining one DAP ply out of phase from the other so that the laminate follows [+ΘDAP(+Λ)/uncoupled substrate/+ΘDAP(−Λ)]. For bending and twist activation, equations (6) and (10) reduce to (12)

$$\begin{bmatrix} B_{11} & B_{12} & 2B_{16} \\ B_{12} & B_{22} & 2B_{26} \\ B_{16} & B_{26} & 2B_{66} \end{bmatrix}_a \begin{bmatrix} \Lambda \\ \Lambda \\ 0 \end{bmatrix}_a = \begin{bmatrix} D_{11} & D_{12} & 2D_{16} \\ D_{12} & D_{22} & 2D_{26} \\ D_{16} & D_{26} & 2D_{66} \end{bmatrix}_l \begin{bmatrix} \kappa_{11} \\ \kappa_{22} \\ \kappa_{12} \end{bmatrix}_l . \quad (12)$$

3.3. Analysis of an antisymmetric 2-DAP ply laminate

Many active structures applications call for control of an uncoupled substrate in bending and twist without cross-feed of bending, κ_{11} to twist, κ_{12}. An antisymmetric laminate with a sequence of [+ΘDAP/uncoupled substrate/−ΘDAP] can control such a laminate without cross-feed.

Twist actuation is obtained by extending both DAP plies so that the laminate has the following structure: [+ΘDAP(+Λ)/uncoupled substrate/−ΘDAP(+Λ)]. For this twist activation, the laminate stiffness matrix of (6) and the actuator stiffness matrix of (10) reduce to another pair of 3 × 3 matrices

$$\begin{bmatrix} A_{11} & A_{12} & 2B_{16} \\ A_{12} & A_{22} & 2B_{26} \\ B_{16} & B_{26} & 2D_{66} \end{bmatrix}_a \begin{bmatrix} \Lambda \\ \Lambda \\ 0 \end{bmatrix}_a = \begin{bmatrix} A_{11} & A_{12} & 2B_{16} \\ A_{12} & A_{22} & 2B_{26} \\ B_{16} & B_{26} & 2D_{66} \end{bmatrix}_l \begin{bmatrix} \varepsilon_{11} \\ \varepsilon_{22} \\ \kappa_{12} \end{bmatrix}_l . \quad (13)$$

This indicates that the simple curvatures κ_{11} and κ_{22} and the shear strain ε_{12} have been decoupled from the twist, κ_{12}.

Bending activation of this laminate is obtained by actuating one DAP element in extension while the other element is in contraction. A sequence of [+ΘDAP(+Λ)/uncoupled substrate/−ΘDAP(−Λ)] shows the stiffness matrices of equations (6) and (10) reducing to another pair of 3 × 3 matrices

$$\begin{bmatrix} A_{16} & A_{26} & 2B_{66} \\ B_{11} & B_{12} & 2D_{16} \\ B_{12} & B_{22} & 2D_{26} \end{bmatrix}_a \begin{bmatrix} \Lambda \\ \Lambda \\ 0 \end{bmatrix}_a = \begin{bmatrix} 2A_{66} & B_{16} & B_{26} \\ 2B_{16} & D_{11} & D_{12} \\ 2B_{26} & D_{12} & D_{22} \end{bmatrix}_l \begin{bmatrix} \varepsilon_{12} \\ \kappa_{11} \\ \kappa_{22} \end{bmatrix}_l . \quad (14)$$

Equation (14) indicates that the twist and simple in-plane strains are not present; the laminate shears and bends in two directions. This ply sequence was used in the experimental models of the following sections.

Since this investigation concentrates on the induction of twist in uncoupled structures, equation (13) is expanded to yield the twist curvature. Equation (15) will be used to estimate the amount of twist that the experimental specimens produce:

$$\begin{aligned} \kappa_{12} = \{&[(A_{11}A_{22} - A_{12}^2)_l(B_{16} + B_{26})_a + (A_{12}B_{26} - A_{22}B_{16})_l \\ &\times (A_{11} + A_{12})_a + (A_{12}B_{16} - A_{11}B_{26})_l(A_{22} + A_{12})_a]\} \\ &\times \{2[(A_{11}A_{22} - A_{12}^2)_l D_{66l} + (A_{12}B_{26} - A_{22}B_{16})_l B_{16l} \\ &+ (A_{12}B_{16} - A_{11}B_{26})_l B_{26l}]\}^{-1}\Lambda. \end{aligned} \quad (15)$$

If the products of the Poisson's ratios are assumed to be approximately equal, ($1 - \nu_{LTa}\nu_{TLa} \simeq 1 - \nu_s^2$) and the DAP elements are attached at ±45° from the longitudinal axis with no bond thickness, then (15) can be solved directly for the twist of the antisymmetric DAP laminate:

$$\begin{aligned} \kappa_{12} &= \frac{(A_{11s} + A_{12s})B_{16a}\Lambda}{(A_{11l} + A_{12l})D_{66l} - 2B_{16a}^2} \\ &= \{(E_s t_s(1 + \nu))(E_{Ta} - E_{La})(t_s t_a + t_a^2)\Lambda\} \end{aligned}$$

Table 2. Activation sequences for generating decoupled strains and curvatures with DAP elements.

Strain or curvature	DAP	CAP	CAP	DAP
		Symmetric		
ε_{11}	0°, $+\Lambda$	$-\lambda$	$-\lambda$	0°, $+\Lambda$
ε_{22}	+90°, $+\Lambda$	$-\lambda$	$-\lambda$	+90°, $+\Lambda$
ε_{12}	+45°, $+\Lambda$	$-\lambda$	$-\lambda$	+45°, $+\Lambda$
κ_{11}	0°, $+\Lambda$	$-\lambda$	$+\lambda$	0°, $-\Lambda$
κ_{22}	+90°, $+\Lambda$	$-\lambda$	$+\lambda$	+90°, $-\Lambda$
κ_{12}	+45°, $+\Lambda$	$-\lambda$	$+\lambda$	+45°, $-\Lambda$
		Antisymmetric		
ε_{11}	0°, $+\Lambda$	$-\lambda$	$-\lambda$	0°, $+\Lambda$
ε_{22}	+90°, $+\Lambda$	$-\lambda$	$-\lambda$	−90°, $+\Lambda$
ε_{12}	+45°, $+\Lambda$	$-\lambda$	$+\lambda$	−45°, $-\Lambda$
κ_{11}	0°, $+\Lambda$	$-\lambda$	$+\lambda$	0°, $-\Lambda$
κ_{22}	+90°, $+\Lambda$	$-\lambda$	$+\lambda$	−90°, $-\Lambda$
κ_{12}	+45°, $+\Lambda$	$-\lambda$	$-\lambda$	−45°, $+\Lambda$

$$\times \{[E_s t_s(1+\nu) + (E_{La} + E_{Ta} + 2E_{La}\nu_{TL})t_a]$$
$$\times [E_s t_2^3(1-\nu)/6 + (E_{La} + E_{Ta} - 2E_{La}\nu_{TL})$$
$$\times (t_s^2 t_a/2 + t_s t_a^2 + 2t_a^3/3)] - \tfrac{1}{2}[(t_s t_a + t_a^2)$$
$$\times (E_{La} - E_{Ta})]^2\}^{-1}. \quad (16)$$

The errors induced in the twist estimation of equation (16) by assuming $(1 - \nu_s^2) \simeq (1 - \nu_{LT}\nu_{TL})$ will be approximately 0% to 5%. A finite thickness bond can also be taken into account by modifying the laminate stiffnesses. For lamina with bond thicknesses one order of magnitude smaller than the thickness of the DAP ply or the substrate, the effects in the bond can generally be neglected.

3.4. Complete decoupling of strains and curvatures

For certain types of vibration and flutter control, complete decoupling of structural strains and curvatures must be achieved. The active structure must be able to generate any strain or curvature without inadvertently generating other strains or curvatures. The following ply sequence [DAP/CAP/uncoupled substrate/CAP/DAP] will be used to achieve this. Table 2 outlines the activation sequence for generating uncoupled strains and curvatures. The constant λ is used to denote a different amount of actuation strain required for the CAP elements. This actuation strain balances the laminate and removes the small amount of adverse strain induced in the laminate from the lateral direction of the DAP elements.

If the directional attachment is ideal, OR = ∞, then the balancing strains, λ, go to zero for generating ε_{11}, ε_{22}, κ_{11} and κ_{22}. For generating pure shear or twist without coupling, the balancing strains must always be present.

This concludes the analysis of DAP and EDAP elements. It should be noted that other types of orthotropic actuators can be analysed by the techniques laid out in equations (5)–(16).

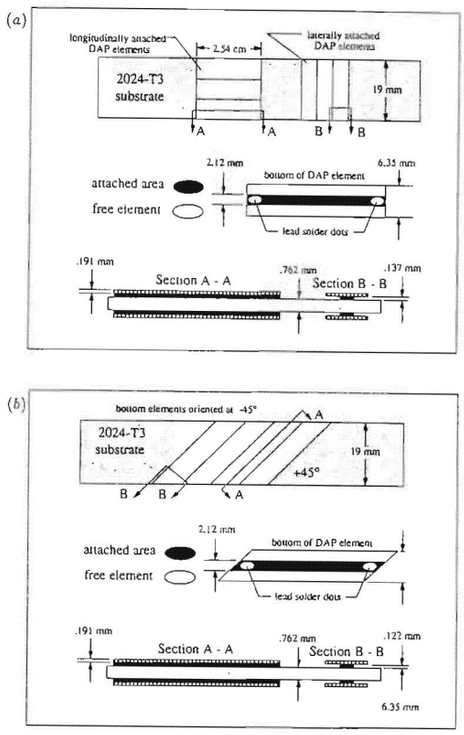

Figure 4. Active beam with (*a*) longitudinally and laterally attached DAP elements, and (*b*) antisymmetrically attached DAP elements.

4. DAP and EDAP specimens

Several types of specimens were constructed to prove the concept of directional attachment and to verify the models that are used to estimate their performance.

4.1. Plate specimens

Three plate specimens were constructed to prove the concept of directional attachment. The first two specimens were constructed from 0.762 mm thick 2024-T3 aluminium with DAP elements laid up at 0°, 90° and $\pm 45°$. They were bonded to the aluminum beams with Hexcel Safe-T-Poxy™ in a room temperature cure. The DAP elements were cut from 0.1905 mm thick G-1195 lead zirconate titanate piezoceramic with nickel electroded faces. Two parting areas were masked off by the presence of a 0.0254 mm thick layer of Teflon between the beam and the DAP elements. This parting strip was removed after the cure to leave the elements free in the lateral directions. The beam geometries are shown in figures 4(*a*) and (*b*).

A direct current signal was applied to each beam and the deflection measurements were taken 15 s after the signal was applied. A laser was reflected off a mirror mounted on the beams and the deflections were recorded.

To verify the directional enhancement models, a fiberglass–epoxy beam was constructed using DAP and EDAP elements. This beam was built on a substrate of

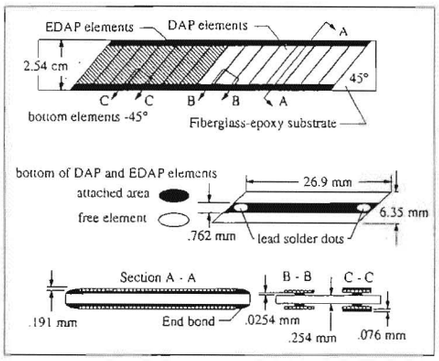

Figure 5. Active beam with DAP and EDAP elements attached antisymmetrically.

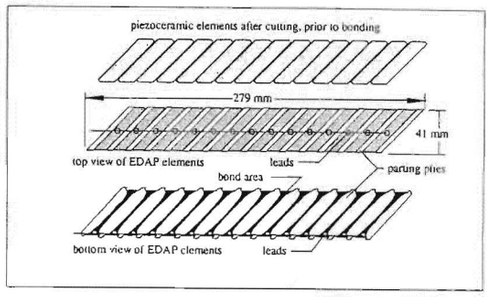

Figure 6. Arrangement of EDAP elements prior to bonding to wing skin.

style # 120 fiberglass cloth oriented along the longitudinal axis of the beam. A wet lay-up using Hexcel Safe-T-Poxy™ was used, with a resulting resin fraction of approximately 45%. DAP elements were applied to the beam at ± 45°. The DAP elements were identical to those used on the aluminum DAP antisymmetric beam. The parting strips were not constructed of 0.0254 mm thick Teflon, but were made from 0.0254 mm thick flashing tape from Airtech corporation. The flashing strips were wrapped completely around the element so as to keep resin from creeping in the space between the elements during the end-bonding. The flashing tape provided a non-stick surface to which the resin could not bond.

Seven of the fifteen elements on either side of the beam also had one ply of Thornel™ P-75s graphite fibers transversely applied to the surface with Devcon five-minute epoxy. The five-minute epoxy has an extremely low modulus which enhances the amount of directional enhancement that is obtained. The geometry of the beam is shown in figure 5.

The DAP/EDAP beam of figure 5 had end-bonds of Safe-T-Poxy placed at the locations where the DAP/EDAP leads were mounted. This end-bonding increased the orthotropy and provided protection for the leads. Like the other DAP beams, the DAP and the EDAP elements were wired in parallel.

4.2. Wing specimens

Two wings were built to further prove the viability of DAP/EDAP technology. The first wing that was constructed had the profile of a 9% thick, graphite/epoxy, diamond shaped supersonic airfoil with an aspect ratio of 3. It had EDAP elements bonded to the underside of the skin and was wired to produce torsional deflections. The second wing was constructed from a DAP torque plate bonded inside of a subsonic missile fin with an aspect ratio of 1.4. This torque plate was strengthened in bending and wired to produce twist deflections.

The supersonic missile wing used EDAP elements bonded on the underside of the skin to induce twist deflections. The skin of the wing was constructed from one ply of Thornel™ P-75s graphite fibers laid up at 45° on the top skin and − 45° on the bottom skin. The skins were laid-up wet with Hexcel Safe-T-Poxy™ in a room temperature cure. The skins had a resin fraction of approximately 40% and were 0.178 mm thick. The EDAP elements were bonded to the surface with a 0.0254 mm thick layer of Hexcel Safe-T-Poxy™ in a room temperature cure.

The EDAP elements had one ply of Thornel™ P-75s graphite fibers transversely applied to the surface with Devcon five-minute epoxy as was done with the DAP/EDAP beam of figure 5.

Two 2k strands of graphite fibers were laid up at the vertices of the skins to provide the wing with bending strength. Care was taken to ensure that the presence of the strands would not interfere with the end-bonding of the EDAP elements. After the skins were cured and the EDAP elements were shear bonded to the skins, end-bonds were formed on the ends of each element. These end-bonds covered the lead junctures and provided added protection from arcing (experienced during high-voltage actuations).

Special attachment patterns were used on the EDAP elements to maximize the amount of longitudinal stiffness and resistance to de-bonding while minimizing the transverse stiffness. It is estimated that the special attachment pattern provided the EDAP elements with orthotropy ratios of approximately 22–25. The parting plies were constructed from 0.0254 mm thick flashing tape. Flashing tape was applied to the tops of the elements to prevent resin creep and to provide jigging stability during parting ply application. The arrangement of the EDAP elements and the parting ply pattern can be seen in figure 6.

The leads were taken from the middle of the elements on the positive poling side and the end of the elements. Layout of the EDAP wing and the location of the leads and the 2k graphite strands are shown in figure 7.

After bonding the two halves of the wing together, the flash at the leading and trailing edges was removed. Polyester end caps were added to the wing. Figure 8 shows the missile wing mounted on a false fuselage undergoing ± 1° twist deflections.

The wing was activated in twist, with signals ranging from 0–200 V DC. The deflections were measured by

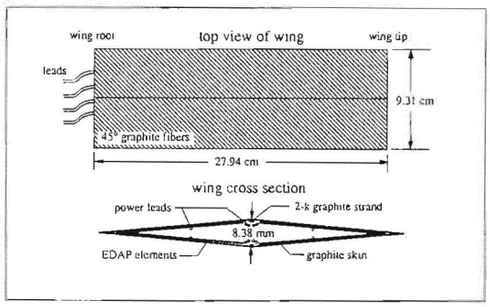

Figure 7. Supersonic EDAP wing geometry.

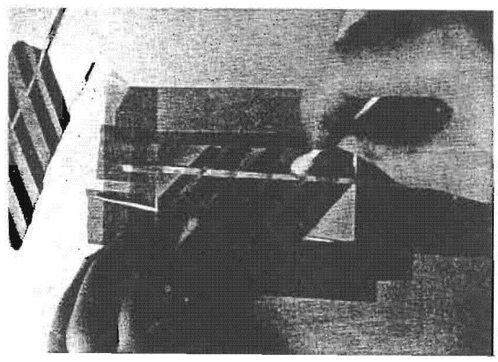

Figure 9. DAP elements during bonding to torque plate.

using a mirror reflecting a laser beam and were taken 15 s after energizing.

The second missile wing used a DAP torsion plate constructed of 10 DAP elements mounted on a 0.127 mm thick AISI 1010 steel plate. The DAP elements were bonded to the surface of the plate with Hexcel Safe-T-Poxy™ in a room temperature cure forming a nominal 0.127 mm thick bond. Flashing tape of 0.0254 mm thickness was used for the parting ply and can be seen in figure 9 mounted on the top side of the DAP elements (the underside pattern is the same as in figure 6).

The DAP elements were soldered together with 0.0254 mm thick brass foil strips as seen in figure 9, with the bottom foil strips being grounded to the plate. A shell of style # 120 fiberglass cloth and epoxy in the shape of an NACA 0010 to NACA 0012 airfoil was constructed as seen in figure 10.

The root of the torque plate is intended to be rigidly attached to a fuselage hard point (for laboratory purposes it is attached to a demonstration stand). The tip of the torque plate is rigidly attached to the inside of the end of the wing as shown in figure 11. A graphite stiffener is added to each side of the wing to give it strength in bending. The stiffener is constructed from Thornel™ P-75s uniaxial fibers and Hexcel Safe-T-Poxy™ bonded in a room temperature cure. The added polar moment of inertia of the stiffener is small with respect to the torque plate and leads to less than a 10% degradation in active twist deflection. The stiffener is placed at the 24% chord. This position places the elastic axis of the torque plate on the 1/4 chord which negates aerodynamic pitching moments. This is critical so that control deflections will be constant with fluctuating airspeeds. (This consistency of control deflection is important as other adaptive flight control devices like piezoelectric ailerons encounter adverse hinge moments which degrade their deflections considerably with increasing airspeed.) The total wing mass is 25.2 g.

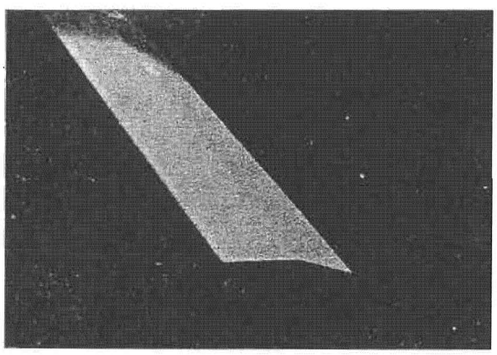

Figure 8. Supersonic missile wing.

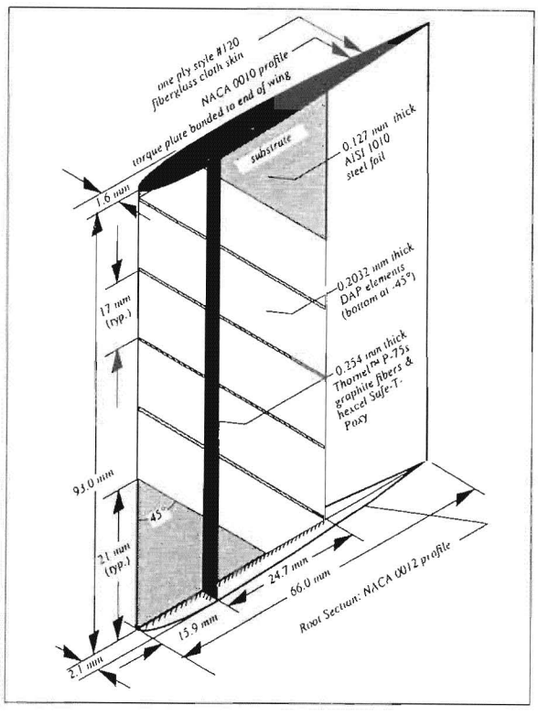

Figure 10. DAP torque plate wing geometry.

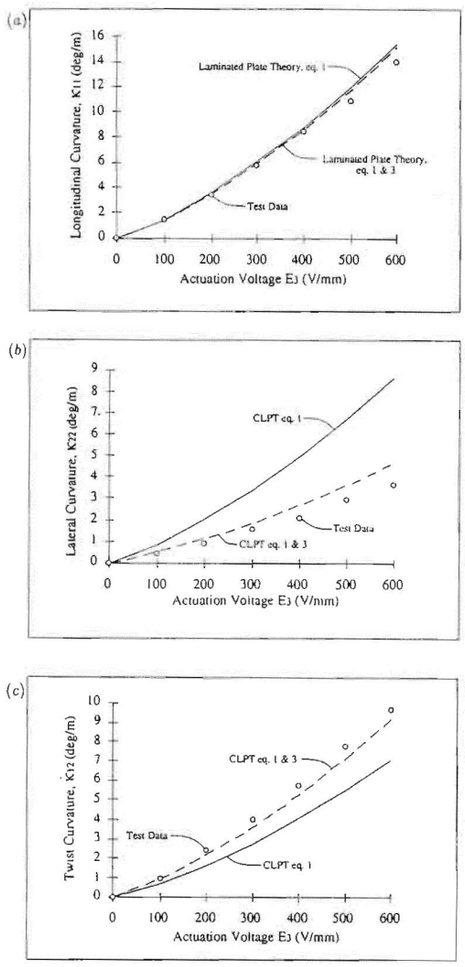

Figure 11. DAP beam bending in (*a*) longitudinal direction, (*b*) lateral direction, and (*c*) DAP beam twist.

5. DAP and EDAP test results

5.1. Plate specimen test results

The deflections of the plate specimens in figure 4 were estimated by equations (1)–(3) and (10). The performance of the plate specimen of figure 5 was estimated by equations (1)–(4) and (10). The resulting effective stiffnesses are as shown in table 3 for the three DAP beams and the DAP/EDAP beam.

The bending and twist deflections of the DAP beams are shown in figures 11(*a*), (*b*) and (*c*). The stiffness estimations of table 3 (from the DAP effective stiffness models) were used in the CLPT predictions shown in figures 11(*a*), (*b*) and (*c*). These models show good correlation in general with experiment. It is thought that the errors are primarily due to inaccuracies in measuring the amount of directional attachment.

From figure 11(*a*), it is obvious that the longitudinal strain reduction due to shear lag is negligible. It is accounted for through equation (3) and shows little modification in the accuracy of the prediction. However, for the lateral stiffness, the inclusion of shear lag is paramount. The inaccuracy of using equation (1) (directional attachment) estimations alone demonstrates that the effective stiffness must be modified by the shear lag estimations of equation (3). In the longitudinal bending case, the accuracy of the prediction methods is good, with an error of less than 8%. For the lateral bending case, the prediction accuracy suffers with an error of 26%. This high error may be due to the degradation of the bond line in the lateral direction.

The twist rate prediction was considerably better than either bending prediction. With an error of 4.2%, the prediction methods used are more accurate than previous methods used by Barrett [11]. The reason that the inclusion of shear lag causes an increase in twist prediction is because the effective transverse stiffness is reduced and accordingly does less work retarding the twist deflection.

Twist deflections on the DAP/EDAP beam were also measured using the same procedures as the DAP beams. The fiberglass–epoxy beam that was used for the prediction of DAP/EDAP performance generated very high deflections which made it necessary to frequently realign the laser beam. These high deflections of the DAP and EDAP portions of the beam are shown in figure 12.

The deflections induced by the DAP elements were predicted with an error of approximately 5%. The analytical predictions of the increase in strain from directional enhancement called for a 13.1% increase in strain from the EDAP elements over the DAP elements, according to equation (4). This increase in actuation strain over the experimentally measured values was actually 8.2%. It is thought that the nearly exact correlation of the EDAP predicted and actual values (error less than 0.8%) is more coincidence than precision in prediction and measurement. It does, however, demonstrate the validity of the prediction techniques.

Using these validated models of directional attachment, the twist deflection of a hypothetical laminate constructed from DAP elements laid up at $\pm 45°$ was compared to the same laminate using conventionally attached elements. This laminate using CAP elements is similar to that used by Crawley and Lazarus [6] and used AS4/3506-1 graphite plies. The graphite, aluminum, and steel substrate plies were $\frac{1}{4}$ the thickness of the piezoelectric plies. This comparison is shown in figure 13 and demonstrates that DAP elements provide up to 16 times more twist deflection than conventionally attached piezoelectric elements on coupled laminates.

5.2. Wing specimen test results

The supersonic missile wing was tested through the full range of deflection. This was done to obtain the full range of data that was available. The half-amplitude deflection was plotted as a function of voltage using DC signals applied for 15 s prior to measurement. The static deflections are plotted as a function of voltage in figure 14.

The data of figure 14 shows that the supersonic wing is capable of twisting $\pm 1°$. Further testing shows that the

Table 3. Properties of DAP/EDAP beam specimens (measurements are in GPa, except t which is in mm).

	E_{Lo}	E_{To}	G_{LTo}	E_{Leffo}	E_{Teffo}	G_{effo}	E_{Leff}	E_{Teff}	G_{eff}	t
Longitudinal and lateral DAP beam										
DAP longit.	63	63	23.7	59.5	21.0	22.4	55.5	11.4	20.9	0.191
DAP lateral	63	63	23.7	58.3	21.0	21.9	53.1	11.4	20.0	0.191
bond	2.9	2.9	1.1							0.137
substrate	70	70	26.3							0.762
Torsion DAP beam										
DAP	63	63	23.7	59.7	21	22.4	56.2	11.5	21.1	0.191
bond	2.9	2.9	1.1							0.122
substrate	70	70	26.3							0.762
Torsion EDAP beam										
piezo	63	63	23.7	57.3	7.56	21.5	56.7	5.2	21.3	0.191
bond	23.4	23.4	8.8							0.025
substrate	23.4	23.4	8.81							0.254
graphite	120	$\simeq 2$	3.6							0.076

wing has a break frequency over 275 Hz with peak amplitudes of $\pm 4°$ at 600 V mm^{-1} actuation potential. No wind tunnel testing was conducted on this model due to budgetary and time constraints, but the aeroservoelastic properties of the wing should yield twist deflections over $\pm 4°$ at $M = 0.7$. These higher deflections are caused by the pitching moments that are generated about the elastic axis (at the 50% chord). Testing of the wing dynamically showed that there are relatively no hysteresis effects from 0 to 100 Hz. Since there are no hinges or frictional linkages present, there is very little structural damping of control motions.

The subsonic DAP wing using the torque plate was also tested for static and dynamic deflection. Predictions of the wing performance were made using the previous estimation equations for the given geometric parameters. The added passive stiffness of the graphite spars was also taken into account by increasing the laminate passive stiffness. The results of static testing up to 750 V mm^{-1} actuation potential are shown in figure 15.

The static wing deflections showed no perceptible hysteresis or stiction as there were no hinges or linkages, only structural damping to dynamically retard motions. The DAP wing had all 10 elements properly poled with no perceptible arcing at the high actuation potentials and no evidence of de-bonds. A demonstration stand was constructed for the testing of the DAP wing. This stand and the DAP wing are shown in figure 16 with the wing undergoing $\pm 2°$ deflections at 90 V DC (443 V mm^{-1}).

These static deflections were measured with a laser beam being reflected off a mirror mounted on the tip of the wing. During dynamic testing (at 600 V mm^{-1}), the participation of a bending mode in the skin of the wing was evident from 35–70 Hz. This bending mode was perceptible in the trace pattern as a Lissajous figure with a maximum eccentricity of 4.5%. It is thought that this bending mode had a negligible influence on the twist results. The active peak-to-peak deflections of the DAP wing are shown in figure 17.

These significant deflections indicate that the DAP wing can be used as a tack-on flight control surface for missiles. To estimate the effectiveness of the DAP wing with respect to other adaptive flight control methods that are available, the performance of the DAP wing was compared to the performance of the piezo flap of [14]. As with the EDAP wing, time and funding constraints made it impossible to test the DAP wing in the wind tunnel. However, an accurate estimate of its performance can still be made. The C_{l_α} of the DAP wing is estimated at 0.104 deg^{-1}. The change in C_l is obtained by using the total pitch deflection and C_{l_α}. The DAP wing static test

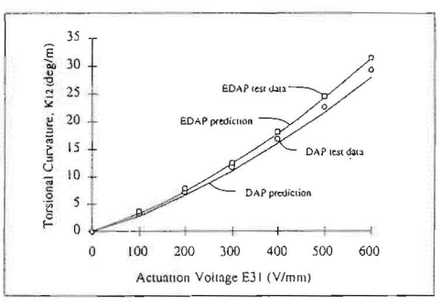

Figure 12. DAP/EDAP beam twist.

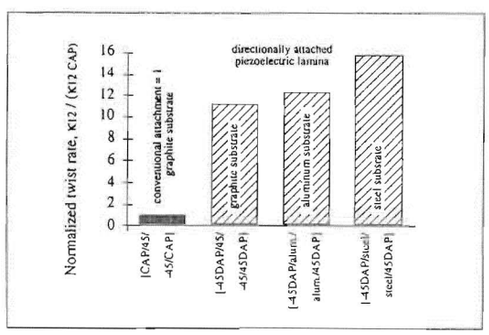

Figure 13. Comparison of active twist rates for conventionally attached piezoelectric (CAP) and directionally attached piezoelectric (DAP) elements.

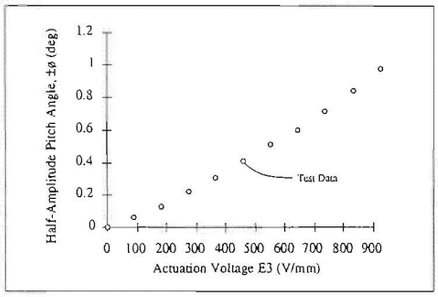

Figure 14. Twist rate of supersonic EDAP wing.

results should be valid for all flight speeds up to approximately $M = 0.7$ (where compressibility effects influence $C_{mac/4}$). This insensitivity to flight speed arises from the characteristics of the symmetrical NACA 0010 and 0012 profiles which have $C_{mic/4} = 0$ for unstalled flight, $M < 0.7$. With no hinges or linkages (which cause a degradation of deflection due to friction), the DAP wing will maintain the same deflections with increasing flight speed. Since the elastic axis of the DAP wing is at the quarter chord, no pitching moment is present.

The performance of the piezoelectric flap is taken from [14] which used a 10% chord flap powered by a bimorph piezoelectric beam. Significant degradations in deflection occurred because of friction in the hinges and linkages. This friction, combined with an adverse hinge moment, caused rapid degradation in the change in lift coefficient. This degradation in C_l was taken directly from [14] at $20\,m\,s^{-1}$ and estimated from the data of [14] at $50\,m\,s^{-1}$. Figure 18 compares this degenerating C_l to the C_l that is maintained by the DAP wing as a function of actuation potential.

6. Conclusions

From the beam experimentation, it can be concluded that there are three ways of achieving directional attachment: partial attachment, transverse shear lag, and differential stiffness bonding. The effective stiffnesses of directionally attached piezoelectric elements can be accurately modeled by an active element area estimation of partial

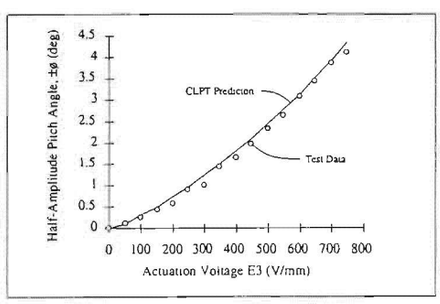

Figure 15. DAP torque plate static deflection.

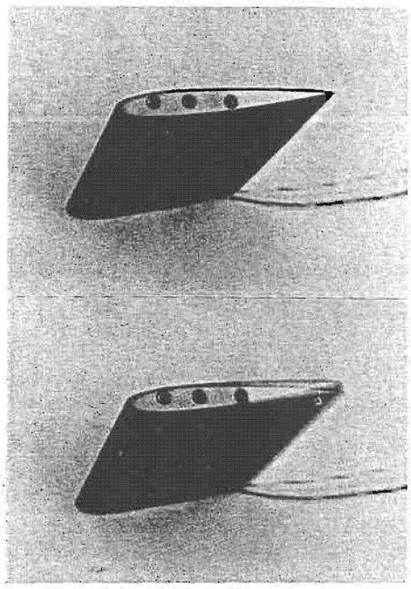

Figure 16. Static and dynamic torque plate wing undergoing ±2° deflections at $443\,V\,mm^{-1}$.

attachment with a shear lag modification. Beams that were constructed with these DAP elements displayed bending rates of $14°\,m^{-1}$, and twist rates of $9°\,m^{-1}$. The analytical models included closed form solutions of strains and curvatures for symmetric and antisymmetric lamina constructed on uncoupled substrates. The analytical models showed good correlation with experiments. The longitudinal bending rate estimations differed from experiment by 8%, and the twist rate models differed by 4.2%. The lateral bending rate estimation (which is of lesser importance to structural applications) differed from experiment by 26%.

The beam experimentation showed that piezoelectric element strains could be increased up to 33% by transverse stiffening of the element with graphite fibers. This directional enhancement was proven on beam specimens

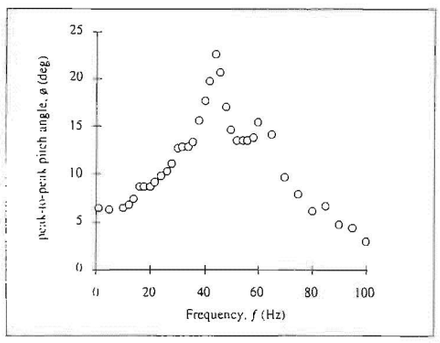

Figure 17. DAP wing pitch amplitude as a function of frequency at $600\,V\,mm^{-1}$.

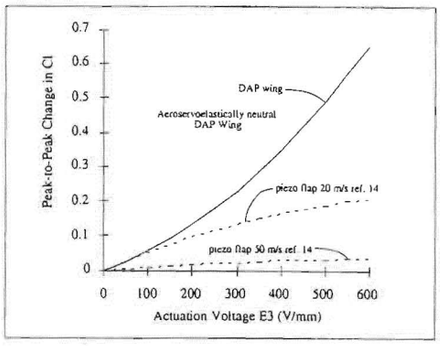

Figure 18. Comparison of piezoaileron [14] and DAP wing active lift coefficients.

with enhanced directionally attached piezoelectric elements and displayed a twist deflection enhancement of approximately 8%. The EDAP beam produced twist deflections of 31° m^{-1} at 600 V mm^{-1} actuation potential. The twist deflections were predicted with less than 1% error.

The models of DAP/EDAP elements showed that lamina could be constructed that produced pure strains, ε_{11}, or ε_{22}, or ε_{12}, and pure curvatures, κ_{11}, or κ_{22}, or κ_{12}, without cross-feeding to any other strain or curvature. For complete decoupling of the strains and curvatures, a 4-ply laminate must be constructed on an uncoupled substrate with: [DAP/CAP/substrate/CAP/DAP]. (It is also possible to imbed the DAP and CAP elements within the uncoupled substrate.) Partial decoupling of actuation strains could be achieved by using only two or three DAP plies.

The analytical models and experiments showed that DAP elements induce up to 12 times more twist than conventionally attached piezoelectric elements on a coupled substrate. Experimentation also showed that conventionally attached piezoceramic elements could produce no twist deflections on uncoupled substrates while DAP elements could produce twist rates in excess of 90° m^{-1} on steel substrates.

A graphite–epoxy substrate was used on a supersonic missile wing that employed EDAP elements as actuators. The wing produced deflections in excess of $\pm 1°$ with a break frequency in excess of 275 Hz.

Pitch deflections in excess of 9° peak-to-peak were measured on a subsonic missile wing that used a torque plate with DAP elements bonded to the surface. Analytical estimations show that the DAP wing produces changes in lift coefficient, ΔC_l, of 0.65 for $M < 0.7$ at 600 V mm^{-1}. This is at least one order of magnitude greater than the ΔC_l available from piezoailerons at flight speeds in excess of 50 m s^{-1}.

Acknowledgments

The author wishes to express his sincere appreciation to the University of Kansas Aerospace Engineering Department for providing laboratory space, and the Kansas Space Grant Consortium, funded by NASA Headquarters, for providing him with support. The author also wishes to acknowledge the support of his wife, Karin, for tolerating the time spent at the laboratory and expenditure of resources to fund this project.

Nomenclature

A = extensional stiffness matrix
B = coupling stiffness matrix
D = bending stiffness matrix
d_{15} = piezoelectric shear-charge coupling coefficient
d_{31} = piezoelectric extension-charge coupling coefficient
d_{36} = piezoelectric in-plane shear-charge coefficient
E = modulus of elasticity
E_3 = actuation potential
G = shear modulus
L = length of DAP element
N = applied force per unit length
M = applied moment per unit length
OR = orthotropy ratio = $E_{L\text{eff}}/E_{T\text{eff}}$
t = thickness
u, v, w = elemental deflections in the x, y, z directions
W = width of DAP element
α = angle of attack
δ = control surface deflection
ε = in-plane strain
ε^0 = mid-plane strain
κ = plate curvature
λ = balancing strain of CAP elements
Λ = free piezoelectric element active strain
ν = Poisson's ratio
Θ = ply orientation angle
σ = ply stress
Ω = actuation frequency

Subscripts
11, 22 ... = tensor notation subscripts
a = actuator
b = bond layer
eff = effective (due to combined attachment methods)
effo = original effective (due to attachment geometry)
l = laminate
o = original (without any attachment effects)
s = substrate

References

[1] Crawley E F and Anderson E H 1989 Detailed models of piezoceramic actuation of beams *Paper presented at the 30th Structures, Structural Dynamics and Materials Conf. (Mobile, Alabama, April 1989)*
[2] Kinsley R S and Budris K 1990 Piezoceramic application data *Piezo Systems Product Catalog* (Cambridge, MA: Piezo Systems, Inc)
[3] Hanagud S 1988 Piezoceramic devices and PVDF films as sensors and actuators for intelligent structures *Paper presented at the U.S. Army Research Office*